Lateral Velocity Anomalies - Model Study

John Toldi

Introduction

We described in SEP-32 (Rocca and Toldi, 1982), a linear convolutional theory that relates perturbations in interval slowness to the resulting perturbations in stacking slowness. The goal of this method is the determination of lateral slowness variations; thus, the ultimate use of the method will be in the inversion of stacking slowness anomalies for the corresponding interval slowness anomalies. As such, this method is intended as an alternative to the linearized traveltime inversion methods, and does not require their often costly and difficult step of determining traveltimes. Instead, stacking slownesses are used -- routine byproducts of a standard seismic processing flow.

In this paper I continue the discussion of this linear theory. The first part of the paper contains a review and discussion of the key points of the theory presented in SEP-32. I present, in the second part of the paper, a depth model containing lateral slowness anomalies. For this model, I derive the stacking slownesses predicted by the linear theory, which I then compare with those derived by fitting ray-trace generated traveltimes. Finally, I present a general discussion of the inversion process, along with the inversion of the ray-trace derived stacking slownesses.

Review of Theory

The derivation of the linear operator relating interval slowness anomalies to stacking slowness anomalies consists of two separate parts (note: $slowness = \frac{1}{velocity}$). The first part is purely statistical: given a particular best least-squares fit line in $t^2 - x^2$ space, determine how the slope of that line (the stacking slowness squared, $= w_s^2$) would change if one of the traveltimes (actually t^2) were changed by a small amount. The second part of the derivation contains the assumptions about the medium: given a medium for which the

stacking velocity is truly the rms velocity (i.e..velocity varies as a function of depth alone, and offsets are not too large), determine the effect on the traveltimes (again actually t^2) of a small localized change in the interval slowness. By connecting the equations derived in these two steps, we obtain the stacking slowness response Δw_s, for a particular reflector at depth z, to an impulse of anomalous interval slowness Δw_{in}, of thickness Δz_{an} and width $\Delta y = midpoint\ interval$, located at depth z_{an}. Finally, by looking at the response to a distribution of such anomalies in midpoint y, we derive the following linear convolutional equation:

$$\Delta w_s(y,z,z_{an}) = \frac{15}{L^2 L'} z\,\Delta z_{an}\left[3\left[\frac{2y}{L'}\right]^2 - 1\right]\left[1 + \frac{L^2}{4z^2}\left[\frac{2y}{L'}\right]^2\right] * \Delta w_{in}(y,z_{an}) \qquad (1)$$

$$= F(y,z,z_{an}) * \Delta w_{in}(y,z_{an})$$

where from Figure 1, $L = cablelength$, and

$$L' = effective\ cable\ length = \frac{(z - z_{an})}{z} L$$

for a constant velocity background. The only change required in the impulse response $F(y,z,z_{an})$ for a depth variable background velocity, is that L' would be a more complicated function of depth.

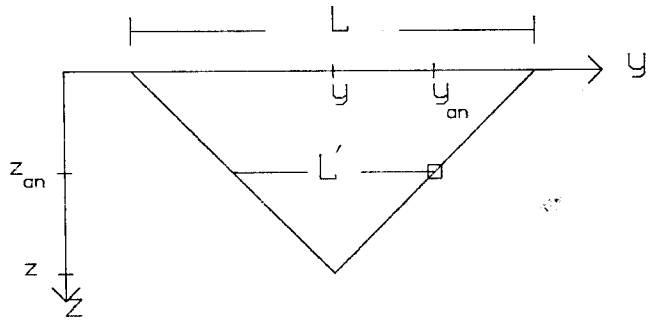

FIG. 1. Geometry for constant background velocity.

Due to the linearity of equation (1), we can simply superpose the contributions of all anomalies from the surface down to the depth of the reflector. Thus, for the anomalous stacking slowness determined for one reflector,

$$\Delta w_s(z,y) = \int_{z_{an}=0}^{z_{an}=z} F(z,z_{an},y) * \Delta w_{in}(y,z_{an})\, dz_{an}. \tag{2}$$

In actually implementing the theory, we cast the problem into the spatial frequency domain. Thus, transforming the impulse response $F(y,z,z_{an})$ over midpoint y to $F(K,z,z_{an})$, then using a dimensionless wavenumber $k = \frac{KL}{2}\frac{(z-z_{an})}{z} = K\frac{L'}{2}$, we find

$$F(z,z_{an},k) = \frac{15z\,\Delta z_{an}}{L^2k^5}\left[\left((2+2c)k^4 + (-34c-6)k^2 + 72c\right)\sin k + \left((6+10c)k^3 - 72ck\right)\cos k\right] \tag{3}$$

where $c = \frac{L^2}{4z^2}$.

$$\Delta w_s(z,k) = \int_{z_{an}=0}^{z_{an}=z} F(z,z_{an},k)\,\Delta w_{in}(k,z_{an})\, dz_{an}. \tag{4}$$

Equations 1,2,3 and 4 were derived in SEP-32 (Rocca and Toldi,1982).

Model Study - Forward Problem

It is interesting to examine how well the operator handles the forward problem, before I proceed to an example of the inversion for interval slowness. The two key assumptions of the theory outlined above are that the anomalies not be too large in magnitude (i.e. the linearization is valid) , and that the hyperbolic moveout relation be valid for the background velocity distribution. In choosing a depth model for this model study, I tried to satisfy these key assumptions: if the theory doesn't work when you do satisfy the assumptions, you can hardly expect it to work in a more general situation.

The depth model shown in Figure 2 is an adaptation from Pollet (1974). The background velocity distribution clearly satisfies the hyperbolic moveout equation, provided the shot to geophone offsets are not taken to be too large. Whether the magnitude of the anomalies is too great for the linearization to still be valid, is not as easily determined. Later in this section, I will show the results derived by increasing the magnitude of the anomalies, which does degrade the fit of the forward problem.

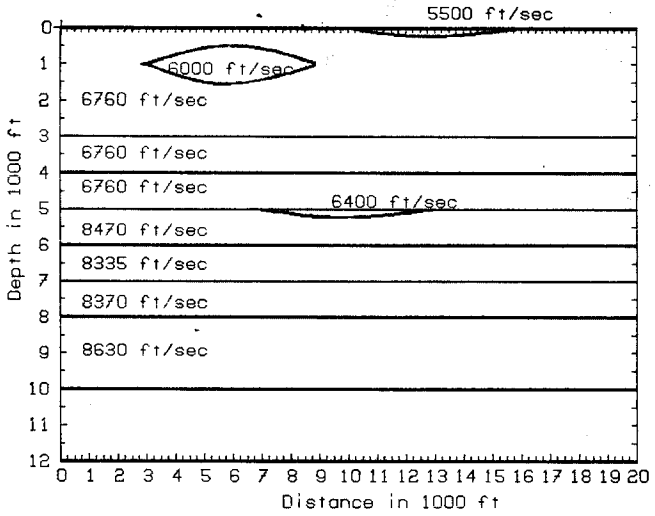

FIG. 2. Depth model containing three low velocity zones. Stacking velocities were determined for the reflectors at depths 3000, 4000, 6000, 7000, 8000, 10000 feet.

Using a ray-tracing algorithm, I generated traveltimes for a standard seismic survey of 16 fold coverage (cable length = 4800 feet) over this depth model. I then determined the stacking slowness for each of the six reflectors by fitting a line in $t^2 - x^2$ space. The stacking slownesses predicted by equation (4) were derived by first forming a grid of anomalous slowness values for the model, [i.e. getting $\Delta w_{in}(y,z_{an})$], performing a Fourier transform over y, then performing the required multiplications and integrations to get stacking slownesses ($\Delta w_s(k,z)$). Finally, with an inverse Fourier transform over k, I get the predicted stacking slownesses $\Delta w_s(y,z)$ for the six reflectors, as a function of midpoint coordinate.

Figures 3 and 4 show a comparison of the ray-trace derived stacking slownesses with the stacking slownesses derived through the linear operator, for two different background velocity distributions. In Figure 3 the operator used a constant velocity background, while in Figure 4 it used a velocity distribution that was linear with depth. For a general depth variable velocity, the effective cable length L' is determined for a particular reflection by tracing the ray corresponding to a shot to geophone offset equal to the cable length L. The ray tracing itself can be done analytically, provided the takeoff angle is known. Only for simple background velocity distributions, such as linear with depth, can this angle be determined analytically; more generally it must be determined through iterative ray-tracing. One such two-point ray-tracing problem would need to be solved for each reflector.

Returning to Figures 3 and 4, we see that either choice of background velocities provides a very good fit with the ray-trace derived slownesses. The differences due to the differing background velocities are largest for the segments of the slowness curves most strongly influenced by the large anomaly at midpoint coordinate 5000, where the depth variable operator clearly provides a better fit.

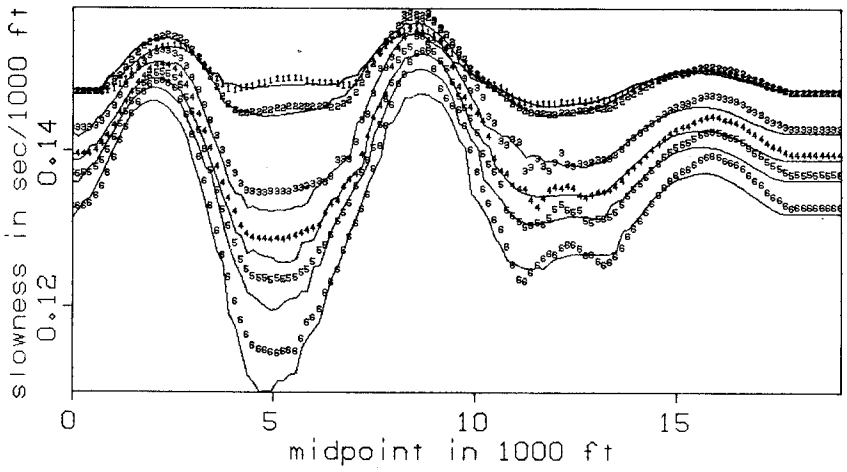

FIG. 3. Two sets of slowness curves determined for the six reflectors of Figure 2. The dotted lines represent the curves determined with the linear operator of equation (3), the solid lines the curves determined by fitting traveltimes from ray tracing. In this figure the forward operator used a constant background velocity.

To study the limits of validity of the linearization, I increased the magnitude of all three anomalies, by decreasing the velocity for each one by 1000 ft/sec. Figure 5 shows the same sort of comparisons as did Figures 3 and 4, namely stacking slownesses derived through ray tracing, compared with stacking slownesses derived through the forward linear operator (here the background velocity was taken to be depth variable). Although the basic shapes of the two sets of curves compared in Figure 5 are still the same (the peaks and troughs occur at the same locations), their amplitudes are clearly quite different. In particular, the fit in the region dominated by the large anomaly at midpoint 5000 feet is much poorer than it was in any region of either Figure 3 or 4. Because the large anomaly differs in velocity from the surrounding material by an amount comparable to that of the other anomalies in the original model, we can infer that the misfit is primarily the result of the magnitude of the anomalous traveltime, rather than the anomalous velocity alone.

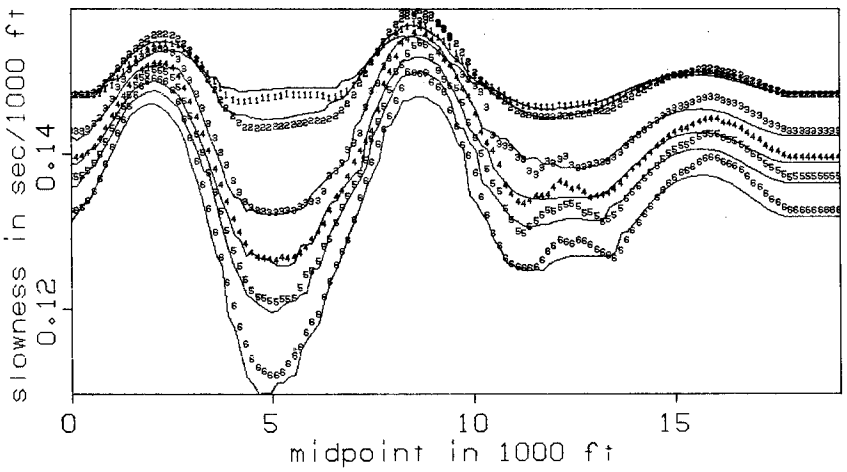

FIG. 4. Two sets of slowness curves determined for the six reflectors of Figure 2. The dotted lines represent the curves determined with the linear operator of equation (3), the solid lines the curves determined by fitting traveltimes from ray tracing. In this figure the forward operator used a background velocity that increased linearly with depth.

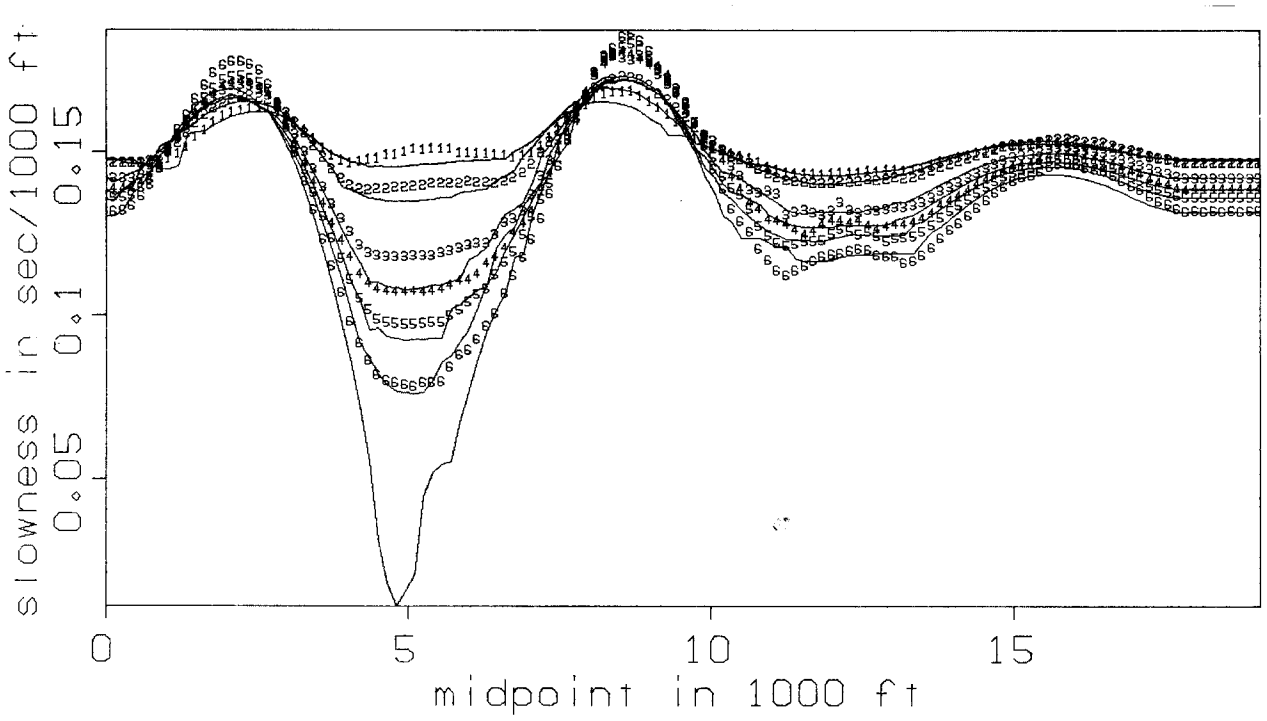

FIG. 5. Two sets of slowness curves determined for the six reflectors of Figure 2, only now with all anomalous velocities decreased by 1000 ft/sec. The dotted lines represent the curves determined with the linear operator of equation (3), the solid lines the curves determined by fitting traveltimes from ray tracing. In this figure the forward operator used a background velocity that increased linearly with depth.

Model Study - Inversion

With the wavenumber k acting as a parameter, there will be one equation like equation (4) for each reflector, that is, an integral of interval slownesses down to the depth of the reflector. Thus, if we replace the integral by a sum, the system of linear equations can be expressed compactly as

$$\Delta\vec{w}_s(z,k) = \mathbf{F}(z,z_{an},k)\,\Delta\vec{w}_{in}(k,z_{an})\,dz_{an}, \tag{5}$$

where now $\mathbf{F}(z,z_{an},k)$ is a matrix operator, with dimensions *number of reflectors* x *number anomalous levels*, and $\Delta\vec{w}_a(z,k)$ and $\Delta\vec{w}_{in}(k,z_{an})$ are vectors.

Because of the existence of zeroes in the operator **F**, and the possibility that we might want to solve for a different number of anomalous levels than reflectors, equation (5) cannot be inverted directly. For the work presented here, I have chosen to form the generalized inverse from the singular value decomposition of **F**. The main advantage to using this method is that it quite easily and naturally allows for control over the eigenvalues in the inversion. Because the matrices involved are really rather small, the usual disadvantage of the method (that the formation of the necessary eigenvalues and eigenvectors can be quite time consuming) is not a serious consideration in the present work.

Following Aki and Richards (1980), we can decompose **F** as follows:

$$\mathbf{F} = (\mathbf{U}_p,\mathbf{U}_0)\begin{pmatrix}\Lambda_p & 0\\ 0 & 0\end{pmatrix}\begin{pmatrix}\tilde{\mathbf{V}}_p\\ \tilde{\mathbf{V}}_0\end{pmatrix}, \tag{6}$$

where **U** and **V** are the eigenvectors of the data and model spaces respectively, $\tilde{\mathbf{V}}$ signifies the transpose of **V**, and Λ_p is a diagonal matrix of nonzero eigenvalues. $\mathbf{U}_0$ is the source of the discrepancy between the observed data and the prediction by the operator **F**, while $\mathbf{V}_0$ is the source of the nonuniqueness in determining the model from the data. The generalized inverse operator is simply

$$\mathbf{F}_g^{-1} = \mathbf{V}_p\,\Lambda_p^{-1}\,\tilde{\mathbf{U}}_p. \tag{7}$$

By limiting the magnitude of the values of Λ_p^{-1}, we can suppress the contributions of eigenvectors with eigenvalue less than a given value. Thus, we can increase the reliability of our results, albeit at the expense of the resolution. The advantage to using the singular value decomposition approach becomes apparent at this point: through the explicit formation of the matrix Λ_p, we can very easily and flexibly control the tradeoff between resolution and reliability.

Before proceeding to the examples of the inversion, I should make one final note. So far, the implication has been that one would want to use all of the wavenumbers in the

inversion. There are both practical and theoretical reasons why one might want to do the inversion only for the smaller wavenumbers. One system of linear equations (of the form of equation (5)) must be inverted for each wavenumber. Thus, from a practical point of view, the execution time can be limited directly by inverting only for a limited number of wavenumbers. Indeed, in the various inversion examples that I attempted, the large wavenumber components of the slownesses were so much lower in amplitude than the small wavenumber components that their contributions were minimal. In addition, ray theory, on which this entire stacking velocity approach is based, is theoretically applicable only when the seismic wavelengths are short compared to the wavelengths of the features being examined. Thus, for the large wavenumber components of the anomalies, diffraction effects, rather than simple traveltime effects, will dominate. In all of the examples which follow, I used only the 30 smallest wavenumbers in the inversion. The largest wavenumber that I used corresponds to a spatial wavelength of approximately 900 ft.

In the first inversion example, I inverted the ray-trace derived stacking slownesses for the original survey (with a cable length, L, of 4800 feet). For easy reference, the depth model is repeated in Figure 6. Note once again that I used the reflections from depths 3000, 4000, 6000, 7000, 80000 and 9000 feet. In this, and all of the subsequent inversion examples, I inverted for 40 anomalous depths. The entire system is thus an underdetermined one (more unknowns than knowns), yet the generalized inverse allows us to extract those components which can be determined.

Figures 7a and 7b are two views of the anomalous interval slownesses resulting from the inversion. The main features of the inversion are quite evident in either view: all three anomalies have been correctly found to have positive slowness (i.e. negative velocity anomalies), and have been properly positioned. While the anomalies are quite well resolved in the lateral direction, they seem to be smeared out in depth between the nearest reflectors. This smearing is particularly evident for the deepest anomaly. In the original depth model it was about 200 feet thick, at a depth of about 5000 feet; in the inverted depth model it is bounded sharply at 4000 and 6000 feet, which are the depths of the nearest reflectors used in the inversion. For the shallower anomalies the depth resolution is not completely determined by the location of the nearest reflectors, although the influence of the shallowest reflector (at depth 3000 feet) is quite evident in Figure 7b. The details of the depth resolution will become much clearer after some of the subsequent examples.

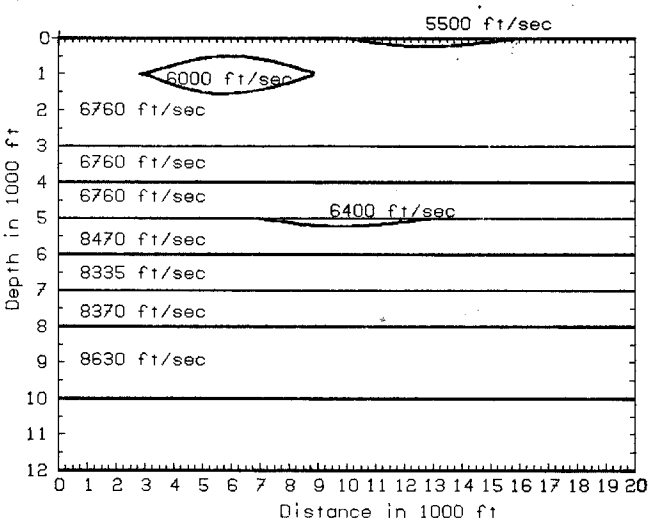

FIG. 6. Depth model containing three low velocity zones. Stacking velocities were determined for the reflectors at depths 3000, 4000, 6000, 7000, 8000, 10000 feet.

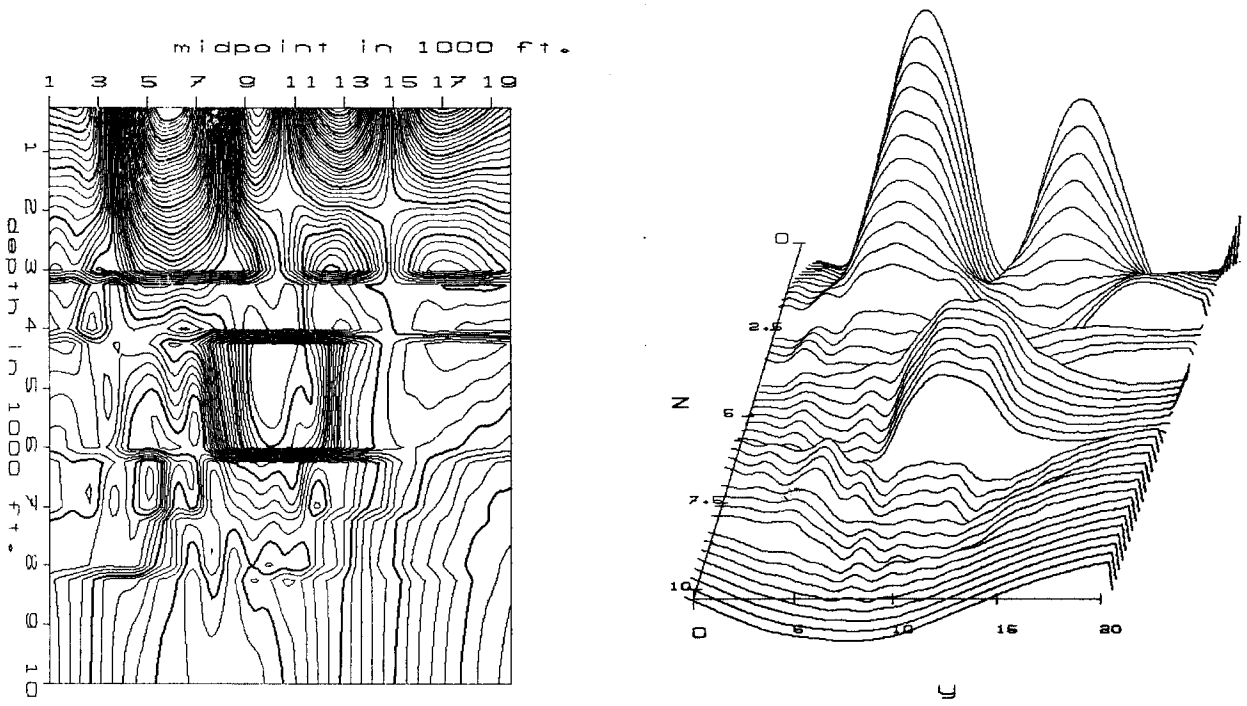

FIG. 7. Anomalous interval slownesses, resulting from the inversion of ray-trace derived stacking slownesses (cable length = 4800 feet). a) Contour plot. b) Hidden line drawing.

The maximum value of Λ_p^{-1} allowed in the inversion must be chosen carefully. This parameter is similar to the stabilization factor commonly found in wavelet deconvolution algorithms. The need for this parameter arises from the fact that components of the model exist that are very weakly passed by the forward operator. Thus, in the inversion, the corresponding components of the data space should presumably be greatly magnified. This would, of course, also greatly magnify any noise present in those components of the data space. Ideally, then, the choice of maximum value of Λ_p^{-1} would be based upon an estimate of the noise level. In practice, we do not know a priori what constitutes signal and what constitutes noise; we thus are lead to an empirical choice of stabilization factor. The specific form of this stabilization or damping parameter that I used was directly tied to the magnitude of the smallest eigenvalue of the inverse problem, i.e. $(\lambda^{-1})_{\min}$. (Note that this eigenvalue corresponds to that eigenvector most easily passed by the forward operator, and hence least in need of magnification in the inversion.) Thus, a damping parameter of .05 means that no eigenvector was magnified by more than 20 times the eigenvector corresponding to $(\lambda^{-1})_{\min}$.

Beginning with Figure 7 and ending with Figure 9, we see the effect of decreasing the damping factor from .075 to .05 to .01. Particularly in going from Figure 8 to Figure 9, we see the appearance of additional peaks of anomalous slowness. Only our knowledge of the original depth model tells us that these peaks are spurious. By decreasing the amount of damping in the inversion, we discover additional features in our inverted depth model; the tradeoff is that we have less confidence in whether these additional features are real. Or, by reversing the argument, we can say that by increasing the amount of damping, we may lose some features, but that we will be more confident of those which remain.

The total cable length L is a very important parameter in this stacking slowness inversion method. Loinger(1983) discussed in detail its implications for the forward problem, the most important being that the anomalous stacking slowness response decreases in amplitude and becomes smoother as the cable length increases. Increasing the cable length also has important implications for the depth resolution in the inverse problem. To study these effects, I once again generated traveltimes by ray-tracing through the depth model of Figure 2, this time with a cable length of 9600 feet (twice the previous value). Figure 10 shows the results of inverting the corresponding stacking slownesses (a damping factor of .075 was used in the inversion). The basic features are much the same as those found with the short cable: all three anomalies have been correctly found to have positive slowness and are properly positioned. The diagonal lines (seen particularly well in the contour plot of Figure 10b), however, were not evident in the short cable examples, nor was the large shallow anomaly near midpoint 5000 feet as clearly resolved in depth as it is here.

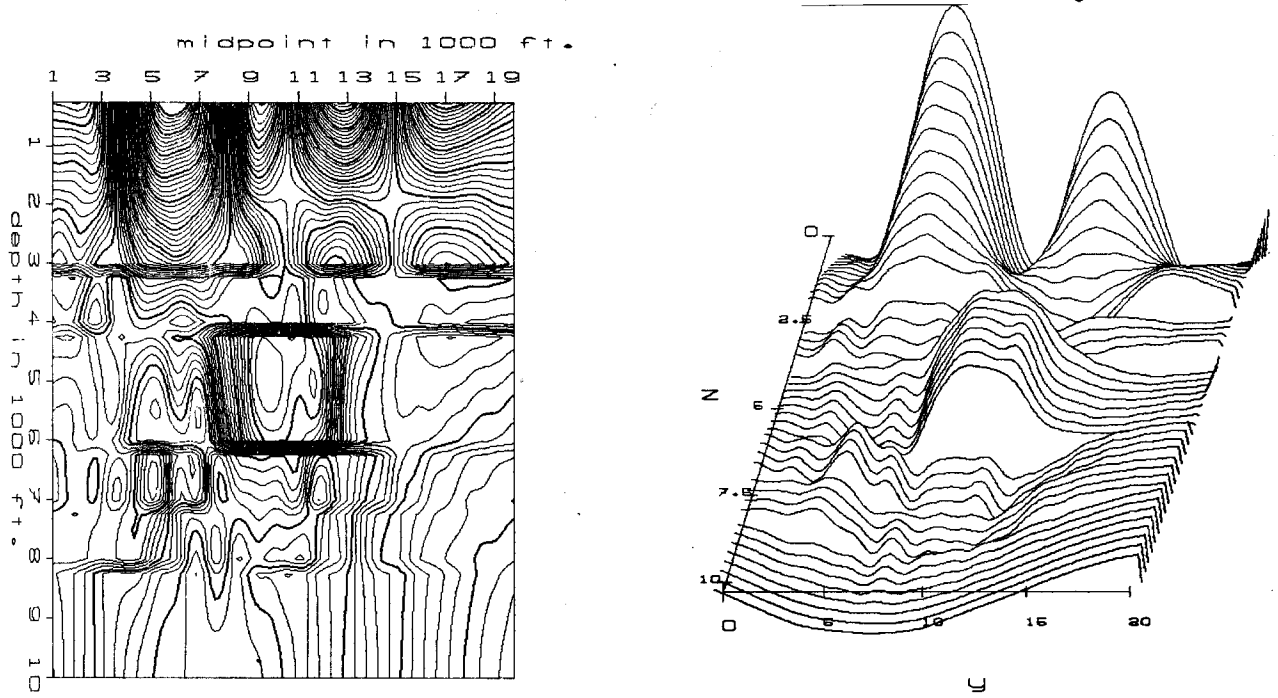

FIG. 8. Anomalous interval slownesses, with damping factor = .05. a) Contour plot. b) Hidden line drawing.

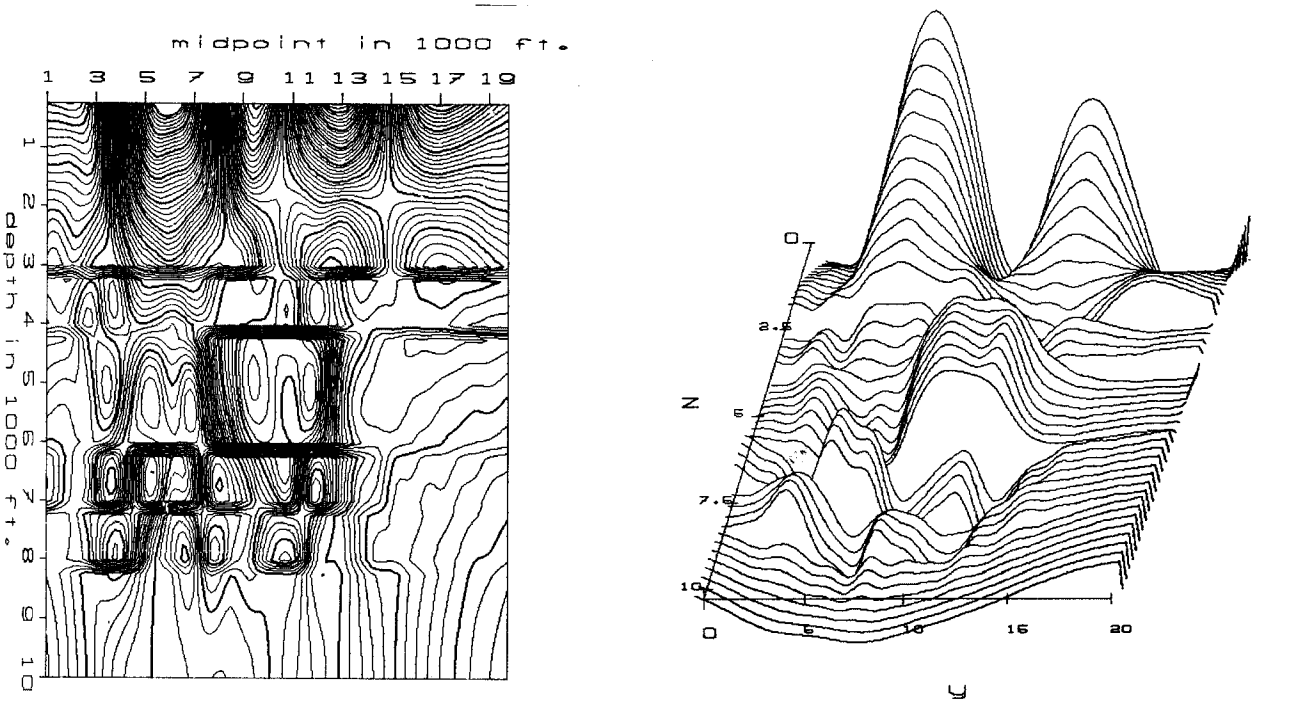

FIG. 9. Anomalous interval slownesses, with damping factor = .01. a) Contour plot. b) Hidden line drawing.

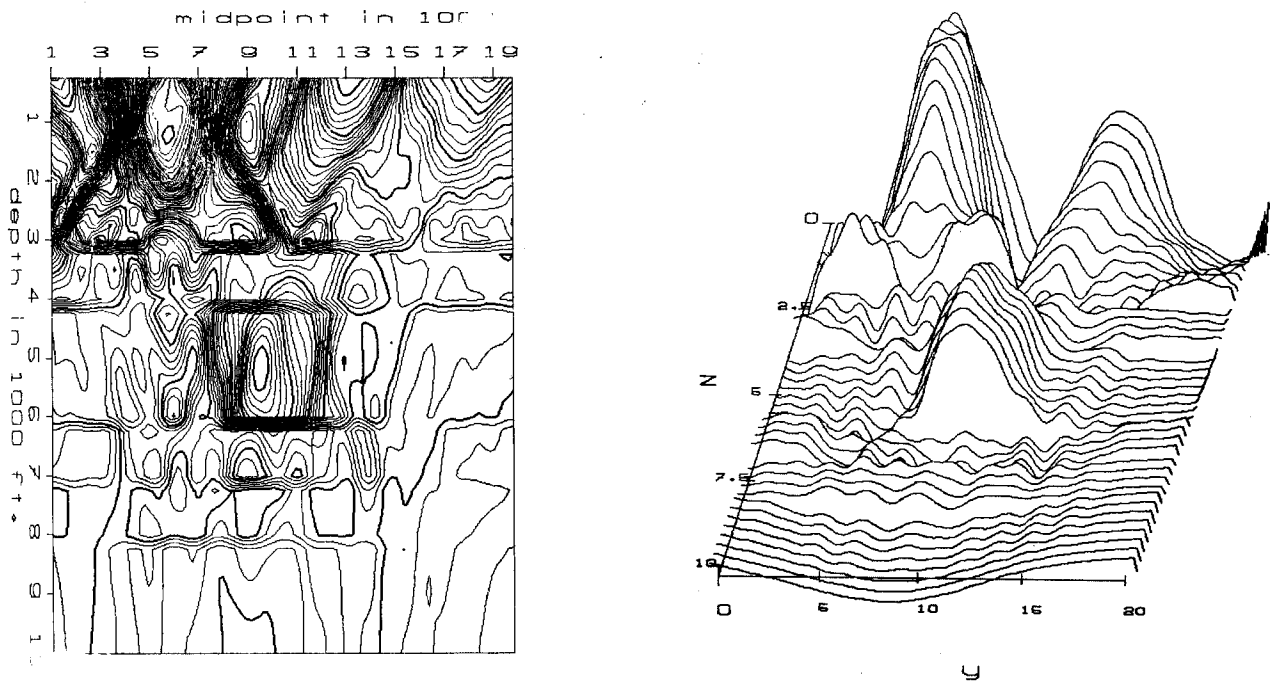

FIG. 10. Anomalous interval slownesses, with damping factor = .075, for cable length = 9600 feet. a) Contour plot. b) Hidden line drawing.

The previous example suggests quite strongly the way in which the depth resolution depends on the cable length. An even more enlightening way to look at this effect, and indeed to gain a better understanding of the depth resolution in general, is to look at the inversion of the stacking slowness curves created through the forward operator. Given the good fit between the ray-trace derived stacking slownesses and those created by the forward operator, we should expect the corresponding inverted results to also resemble one another closely. As will be seen presently, this is certainly the case. On the other hand, by focusing our attention on the results of running the operator forward, then backward, we can be more certain that we are looking at the intrinsic limitations of the operator itself.

Thus, Figure 11 shows the results of inverting the slowness curves derived through the forward operator, for a cable length of 9600 feet. A comparison with Figure 10 shows that the inverted interval slownesses are indeed much the same as those derived from the ray-trace results. Aside from the obvious difference that the results of inverting the forward operator data are less noisy, the most notable new feature of Figure 11 is the absence of the any buildup of amplitude between depths 7000 and 8000 feet. (Compare particularly the contour plots ,Figures 10a and 11a). Thus, when the data fit the model perfectly, the inverse operator is able to limit the anomalies to be between the appropriate reflectors. In the more realistic case of the data fitting the model only approximately, some components of

the data will seem to the inverse operator to be consistent with anomalous interval slowness at other depths (e.g. the extra amplitude in the interval slownesses of Figure 10 between 7000 and 8000 feet).

The strong diagonal lines first seen in Figure 10 are also clearly evident in Figure 11. Particularly striking is the "v" pattern, which outlines the bottom of the large shallow anomaly at midpoint 5000 feet. This effect quite clearly arises from the existence of raypaths which entirely undershoot the anomaly. Because such raypaths sense no anomalous material, they provide a boundary to the region which contains the anomaly. The effect is further clarified by returning to the short cable experiment. Figure 12 contains the results of inverting the forward operator derived stacking slownesses for a cable length of 4800 feet. Here the cable is simply too short too allow any undershooting of the anomaly, thus the absence of the clear "v" pattern. What resolution there is of the lower limit of the anomaly comes from the raypaths which have, for example, the downgoing leg traveling diagonally under the anomaly, but then the upgoing leg necessarily traveling through the anomaly. The net result is that the bottom of the anomaly gets bounded by a more steeply dipping and less sharply defined line.

A similar story applies to the resolution of the top of this large shallow anomaly. For the long cable case (Figure 11) there are raypaths which travel entirely above the top of the anomaly. Thus, precisely as for the bottom of the anomaly, these raypaths will have sampled no anomalous material, the net effect being improved resolution of the top of the anomaly. For the short cable case (Figure 12), there is no such constraint on the top of the anomaly. Indeed, a glance at the original depth model (Figure 6), shows that the anomaly is so shallow and broad that there is a region, for the short cable case, that is not sampled by any raypaths which do not also pass through the anomaly. The resulting effects are quite easily seen in Figure 12: the anomaly has a central region which is bounded above only by the surface.

The same raypath considerations apply equally well to the other two anomalies. The shallowest anomaly has a somewhat squarer shape for the short cable than it does for the long cable. Once again, this can be attributed to the short cable experiment's lack of raypaths slanting closely under the anomaly. For the deepest anomaly, the effects are more subtle. For either choice of cable length, the basic shape is the same: the anomaly has nearly vertical side boundaries, and is bounded above and below by the reflectors at 4000 and 6000 feet respectively (recall that the reflector at depth 5000 feet was not used). Neither of the cables is long enough to provide raypaths which deviate far from vertical for a reflector at this depth. This clearly results in nearly vertical sides for the inverted anomaly.

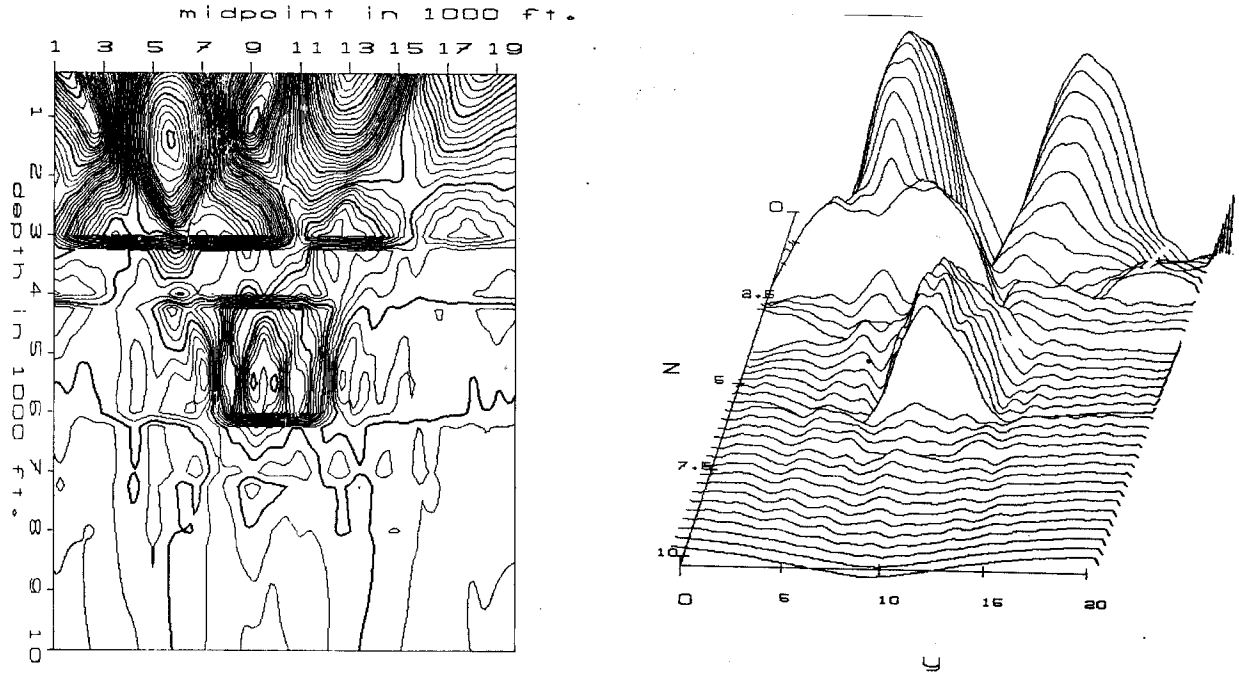

FIG. 11. Anomalous interval slownesses, resulting from the inversion of stacking slownesses from the forward operator, for cable length = 9600 feet. a) Contour plot. b) Hidden line drawing.

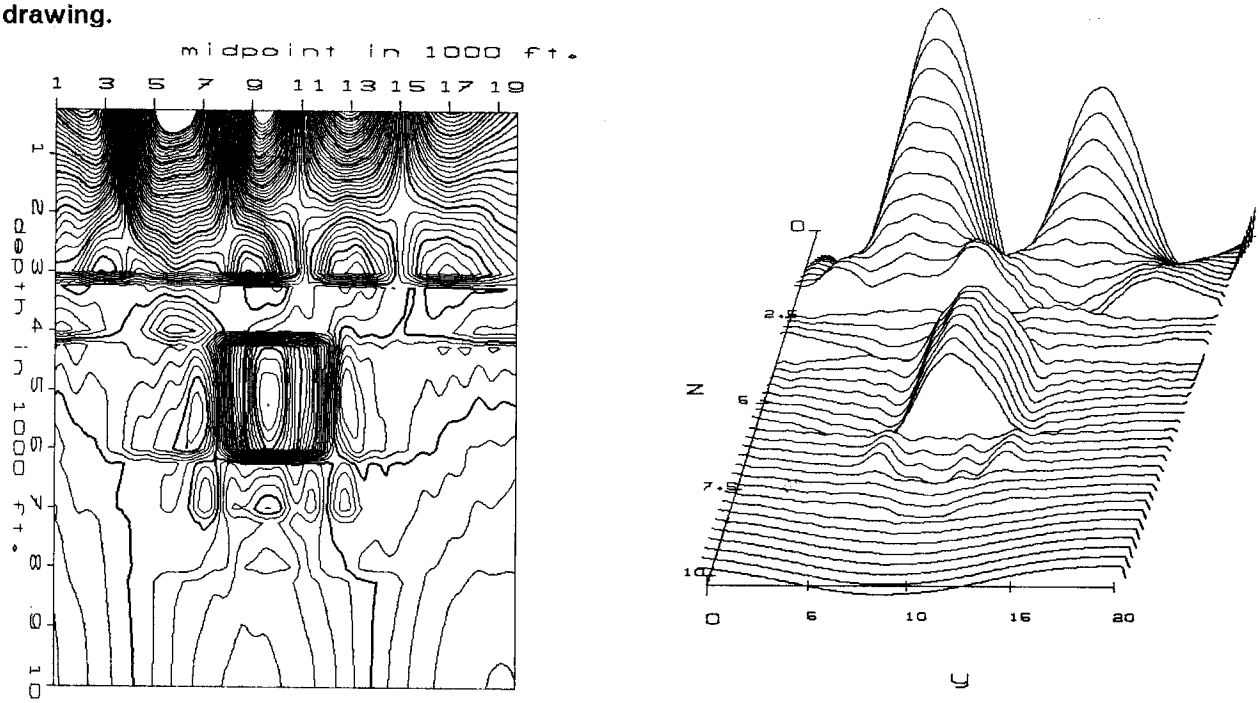

FIG. 12. Anomalous interval slownesses, resulting from the inversion of stacking slownesses from the forward operator, for cable length = 4800 feet. a) Contour plot. b) Hidden line drawing.

We can, however, carry the analysis somewhat beyond a discussion of the basic shape of this deep anomaly, and look at some of its finer details. Whereas the anomaly derived from the short cable experiment has truly vertical sides, the anomaly for the long cable exhibits a broadening with depth. This agrees well with the fact that the anomaly actually began below 5000 feet in the original depth model.

Although the discussion of the depth resolution dealt with the results derived through inverting the output of the forward operator, a glance through the earlier ray-trace derived examples shows that they contain most of the same features. It is interesting that raypath considerations were so successful in explaining the observed results, in that precisely the same considerations would apply to a discussion of the resolution of anomalies in a travel-time inversion. Thus, even though the stacking slownesses are a statistical average of the traveltimes, we are able to extract the same information about the depth distribution of slowness as from the traveltimes themselves.

REFERENCES

Pollet, A., 1974, Simple velocity modeling and the continuous velocity section: Paper presented at the 44th annual meeting of the Society of Exploration Geophysics, Dallas, Tx.

Aki, K., and Richards, P., Quantitative seismology: San Francisco, W.H Freeman, 1980.

Rocca, F. and Toldi, J., 1982, Lateral velocity anomalies: SEP 32, p.1-13.

Loinger, E., 1983, A linear model for velocity anomalies, Geophysical Prospecting, v.31, p.98-118.

FROM: R. E. DuBROFF
285 GB, PHILLIPS PETROLEUM
BARTLESVILLE, OK. 74004

TO: PROF. JON F. CLAERBOUT
DEPT. OF GEOPHYSICS
STANFORD UNIVERSITY
STANFORD, CAL. 94305

RE: SEP #30, #32

THE SECTION ON ROTTEN ALLIGATORS CONJURED UP THIS IMAGE IN MY MIND.

R.E.D

Rotten alligator, indeed!